Nanotubes in Nanoelectronics: Transport, Growth and Modeling

M. Anantram, Lance Delzeit, Alan Cassell, Jie Han, and M. Meyyappan*
NASA Ames Research Center
Moffett Field, CA 94035 USA

Carbon nanotube (CNT) based nanotechnology appears to be promising for future nanoelectronics. Theoretical analysis and results for the ballistic current carrying capacity of nanotube wires are presented. Aspects of metal-nanotube coupling are examined. Results are also presented for chemical vapor deposition of CNT from hydrocarbon feedstock.

* Corresponding author – (650) 604-2616 (Phone), (650) 604-5244 (Fax), meyya@orbit.arc.nasa.gov

Introduction

Current generation silicon CMOS devices have a gate size of 0.25 microns while research is active to reduce the feature size to 0.18 and 0.13 microns. It is expected by 2007, the feature size will be below 0.1 micron (100 nm). At feature sizes smaller than 100 nm, problems due to physics may arise, preventing successful operation of the device; even if this is not the problem, manufacturing problems may prevent realization of devices smaller than 100 nm feature size. The manufacturing problems include viable lithography technique, interconnects, and many other aspects of integrated circuit production. As a result, there has been activity in the areas of alternative device structures, architectures, quantum and other novel computing techniques. Some of these research efforts are expected to come into fruition in the next 20 years when the silicon engine may potentially run out of steam.

Nanotechnology is receiving much attention for the possibility to develop inexpensive, 'bottom-up' manufacturing techniques as opposed to the present 'top-down' miniaturization [1]. Carbon nanotube (CNT) based nanotechnology appears to be promising for future nanoelectronics. The CNT is an elongated fullerene and is a long tube compared to its diameter. It can be thought of as a two dimensional graphene sheet

rolled into a tube. Depending on how the rolling is done, the CNT may be either metallic or semiconducting. Indeed, both metallic and semiconducting types of CNTs have been observed experimentally. This gives rise to intriguing possibilities to put together semiconductor-semiconductor and semiconductor-metal junctions, and diodes, and transistors [2]. CNT is also being investigated as a field emitter source for flat panel display applications [3].

The potential for nanotubes in nanoelectronics, displays, nanosensors and devices is enormous. However, the challenges ahead are also numerous. Controlled growth on patterned substrates, control of nanotube chirality, diameter and properties, characterization, development of nanoelectronics and computing building blocks and architectures pose some of the challenging issues. In this paper, some recent results on growth as well as computational modeling of transport issues in nanotubes are presented.

Carbon Nanotubes: An Overview

Nanotube structures arise by rolling a graphene sheet into a cylinder in a way that the lattice points fold onto each other. The structures are uniquely defined by a lattice vector $\mathbf{c} = n\mathbf{a} + m\mathbf{b}$ where **a** and **b** are the atomic lattice unit cell vectors and n and m are two integer indices. It has been shown that when (n-m)/3 is an integer, then the nanotube is metallic; otherwise it is a semiconductor [4]. The bandgap is given by $E_g = 2\gamma_o a_{c-c}/d$ where a_{c-c} is the C-C bond length, d is nanotube diameter and γ_o is the near-neighbor hopping parameter. Electronic properties can be tailored through application of an external magnetic field, introduction of mechanical deformation or creation of structural defects. These intriguing electronic properties provide an opportunity to create metal-semiconductor and semiconductor-semiconductor junctions which would lead to functional devices. In order to realize this potential, it is critical to understand how manipulation of the nanotubes affects the bandgap. Theoretical work combining molecular mechanics, dynamics and tight binding calculations has been used to study the effect of uniaxial deformation and torsion on the CNT electronic properties [5]. Uniaxial tension or compression has no effect on arm chair (5, 5) tubes whereas in other cases the nature of change in bandgap with uniaxial strain depends on the chiral angle. For example, the bandgap change with strain is stronger for a (10, 0) tube than for a (6, 5)

tube. In general, three types of transitions have been observed [5]: (1) metal-semiconductor transition, example (9, 0) tube at 1% strain, (2) dE/d (strain) changes sign due to quantum number change, example (10, 0) at 10% strain; and (3) dE/d (strain) changing sign due to mechanical relaxation, example, (10, 0) tube at 18% strain. Similar quantifications have also been done for the effect of torsion. Beyond electronic properties, the effect of vacancies and disorders on the conductance of nanotube quantum wires also has been modeled [6]. Theoretical work leading to the organization of T and Y junctions involving metallic and semiconducting nanotubes has been presented by Menon and Srivastava [7] which can lead to interesting logic gate arrangements. Indeed, this concept was recently verified by transport measurements on Y-junction nanotubes [8]. The experimental results show intrinsic nonlinear transport and reproducible rectifying behavior. Prior to this, demonstration of transistor effect in nanotube-based FET-like devices has been made by Tans et al [9] and Martel et al [10]. Among various nanowires, the largest current to this date can be driven through CNT: a small bias resistance of 12.5 kΩ [11] has been recorded through a multi-wall nanotube. This resistance is only twice the theoretical minimum of 6.25 kΩ through a single wall of a nanotube. Reference 12 demonstrated a resistance as small as 500 Ω in a sample making contact to many layers of a carbon nanotube.

Growth of Single-Walled Nanotubes

Growth of single-walled nanotubes (SWNT) has been primarily accomplished by laser ablation or carbon arc techniques. The product typically consists of SWNT along with catalyst metal particles and amorphous carbon. Purification techniques have been developed to isolate SWNT from the product and previous device demonstrations [9, 10] have used purified SWNT to fabricate FET-like structures as well as in current transport studies. As it is difficult to handle nanotubes to make devices as in references 9 and 10, it is important to develop approaches to grow SWNT on patterned substrates which can lead to device integration. In this regard, chemical vapor deposition seems to be an ideal technique for growing nanotubes on patterned substrates [13].

Our CVD approach uses hydrocarbon feedstock (methane or ethylene) at temperatures 700-900° C at atmospheric pressure. SWNT growth requires a transition metal catalyst which we have been able to deposit on silicon substrates either from solution or by physical sputtering. The spot size by the solution technique is always larger than by physical sputtering. The nanotube diameter depends on the catalyst particle size. Therefore, the catalyst deposition technique, particularly the ability to control the particle size and keep the catalyst particles faithfully within patterns, is critical to developing nanodevices. Progress on this front is slow. Figure 1 shows a transmission electron micrograph of a SWNT grown by CVD. Our current work focuses on correlating catalyst particle size to nanotube properties and developing device-specific processing steps.

Bragg Reflection in Carbon Nanotube Wires

At the band center of a metallic carbon nanotube, there are two sub-bands. When coupling to contacts is perfect and in the absence of defects, this will yield a minimum resistance of 6.25 kΩ at small voltages. At large applied voltages, electrons are injected into numerous sub-bands. For example, there are more than 25 sub-bands in a (30,30) armchair nanotubes at an energy of 2.5eV (The number of sub-bands available for transport off band center typically decreases as inverse of the carbon nanotube diameter.). If all these sub-bands contribute to current, the differential resistance due to a single nanotube layer can be as small as 500 Ω. Contacting many layers will yield an even smaller resistance. Scattering mechanisms due to defects and phonons will reduce the resistance. In this section, we address the issue of an intrinsic mechanism that limits the current carrying capacity of a CNT that plays a role even in a defect and phonon free situation.

We consider the truly metallic armchair nanotubes and assume perfect carbon nanotube leads. The calculations are within the context of a pi orbital per carbon atom with the nearest neighbor hopping parameter equal to 3.1 eV. We calculate the single particle transmission probability and current by the procedure in reference 6. Thus true many body effects such as in Luttinger liquids are neglected [14]. In a current versus voltage calculation it is important to take the potential drop across the nanotube into account. This should in principle be determined by the self-consistent solution of Poisson's

equation and a quantum mechanical procedure to calculate the non equilibrium electron density, which is a difficult problem for nanostructures. We believe that to convey the essential physics, plausible potential drops across the nanotube are sufficient. The potential drop [V(x)] is an input to the Hamiltonian and is modeled by changing the on-site potential. The assumed functional form for V(x) is,

$$V(x) = \frac{V_a}{2}\left\{1 + \frac{1+e^{\frac{L}{L_{sc}}}}{e^{\frac{L}{L_{sc}}}e^{\frac{L}{L_{sc}}}}e^{-\frac{x}{L_{sc}}} - \frac{1+e^{\frac{L}{L_{sc}}}}{e^{\frac{L}{L_{sc}}}-e^{\frac{L}{L_{sc}}}}e^{\frac{x}{L_{sc}}}\right\} \qquad (1)$$

where V_a is the applied voltage, L is the length of the nanotube, L_{sc} is a parameter that determines the nature of the voltage drop and x is the nanotube axis. $L_{sc} > L$ implies a linear voltage drop. The voltage drop in quasi 1D structures is expected to have a more gradual dependence than the exponential drop in Eq. (1). So the chosen dependence is a conservative one. In choosing L_{sc} we are guided by theoretical calculations, which have yielded reasonably large screening lengths even for armchair tubes [15]. The results presented below for the (10,10) nanotube however do not change significantly over the range of (25-200 $\AA$) considered. The current is computed using the Landauer-Buttiker formula,

$$I = \int dE T(E)[f_L(E) - f_R(E)] \qquad (2)$$

where, T(E) is the transmission probability, and $f_L(E)$ and $f_R(E)$ are the Fermi factors in the left and right contacts respectively.

We first focus on the defect free case ('no defect' of Fig. 2). The surprising feature here is that the maximum conductance is only $4e^2/h$. This conductance is equal to the value obtained if only two sub-bands conduct. Note that for a (10,10) nanotube, the first non crossing sub-band opens at around 0.85eV. It is clear from the $[f_L(E) - f_R(E)]$ factor of Eq. (2) that this means that electrons injected into this sub-band can carry current at an applied voltage of 1.7V if the transmission probability is larger than zero. There is however *no* indication of an increase in the differential conductance in Fig. 1. What happens to the electrons injected into the non crossing sub-bands of the nanotube? The answer to this issue can be understood by considering the semiclassical picture of electron flow from the left to the right contact. Fig. 3 is a plot of the $E_n(k)$ relationship of a nanotube at different positions along the length, where *n* is the sub-band index. The sub-band centers at the left and right ends of the nanotube are at voltages of V_a (the applied voltage) and zero respectively. For $V_a < 3.1V$, an electron injected from the left contact in between the Fermi energies of the right (μ_R) and left (μ_L) contacts in the two available crossing sub-bands flow to the right contact unimpeded. In contrast, the reflection probability of an electron injected into a non crossing sub-band is large. The wavevector evolution under the influence of a static electric field [F(r)] is given by,

$$\frac{1}{\hbar}\frac{dk}{dt} = -eF(r) \text{ and } v_n(k) = \frac{1}{\hbar}\frac{dE_n(k)}{dk} \qquad (3)$$

The wavevector of an electron injected from the left contact into a non crossing sub-band (n) increases, as the electron propagates to the right in Fig. 3. The velocity $v_n(k)$ in sub-band n is zero at the sub-band extrema, which defines the location of Bragg reflection. The dotted horizontal line is an example of an electron injected from the left contact into a non crossing sub-band, which undergoes Bragg reflection at the location of the arrow. It can be seen that such a reflection also occurs in all other non-crossing sub-bands. As a result, the non crossing sub-bands do not contribute to current and the maximum differential conductance is approximately $4e^2/h$. Alternately, in Fig. 3, a horizontal line at any given energy in between μ_R and μ_L passes through a region where *only* the crossing sub-bands are present. An electron incident into a *non-crossing* sub-band at this energy can reach the right contact *only* by passing through a region where only the *crossing* sub-bands are present. Hence in the absence of either significant inter sub-band or inelastic scattering, they must be reflected. In the 'no defect' case of Fig. 2(a), the current plateaus out for voltages larger than 3.1V and this leads to a differential conductance that is close to zero [Fig. 2(b)]. Applying a voltage larger than 3.1 V leads to electrons in some energy ranges being Bragg reflected, while new energy ranges contribute to transport. They conspire in a manner so as to keep the total current constant in the voltage range shown.

The effect of two other relevant mechanisms that lead to differential conductances larger than that shown by the solid line in Fig. 2 are now calculated. They are defect scattering and inter sub-band tunneling. We model defects by a random change in on-site potential as discussed in Ref. 6. From a physical view point, Bragg reflection of electrons incident in the non crossing sub-bands will be weakened as electrons have a non zero probability

to reach the right contact by defect aided scattering to right moving states in sub-bands other than the incident one. The results of calculations that fully account for such processes are shown in Fig. 2. The differential conductance is clearly larger in the presence of defect scattering at larger voltages for reasons just discussed. The absolute value of current can be larger or smaller than in the 'no defect' case and this depends on the extent of defect scattering. Clearly, large defect scattering leads to currents smaller than in the 'no defect' case. An important point here is that the differential conductance remains smaller than the small bias values. This is because an electron incident into a *non-crossing* sub-band from the left contact between μ_R and μ_L can reach the right contact *only* by passing through a region where only the *crossing* sub-bands are present. This results in a bottle neck for driving current commensurate with the number of sub bands into which electrons are injected.

We now present results concerning the role of Zener type inter sub-band scattering in the absence of defects [16]. If most of the applied voltage drops across short lengths of the tube such that the electric field is large, inter sub-band tunneling will aid in leading to larger differential conductances *even* in the absence of defect scattering. The distance over which an electron should tunnel before reaching the next sub-band in the presence of an electric field will depend on the energy spacing between sub-bands. The energy level spacing decreases (ΔE_{NC} of Fig. 3) with increase in nanotube diameter. So, the Zener tunneling probability increases with increase in diameter. This is illustrated in Fig. 4, which shows the current versus applied bias for nanotubes of various diameters. The data for Fig. 4 was computed by assuming that the applied voltage drops uniformly over a

distance of 10Å. The (20,20) nanotube has the smallest ΔE_{NC} (approximately 0.9 eV) amongst these nanotubes. The Zener tunneling current is correspondingly the largest. The (5,5) nanotube has ΔE_{NC} corresponding to 3.4eV, and so Zener tunneling is absent because of the large barrier to tunneling.

In summary, in the case of perfect contacts and absence of defects, there are three possibilities for an electron injected from the left contact (Fig. 3): (i) Direct transmission: an electron is transmitted in the injected sub-band as shown by the solid line, (ii) Bragg reflection: reflection that occurs when the wave vector (k) of an injected electron evolves to a value where the velocity in sub-band n, $v_n(k) = 0$. An electron undergoes Bragg reflection at the location of the arrow corresponding to the dotted line, and (iii) Inter sub-band Zener type tunneling: tunneling between sub-bands induced by an electric field. The spacing between non crossing sub-bands (ΔE_{NC} of Fig. 3) decreases inversely with increase in nanotube diameter. So, Zener tunneling should become increasingly important in determining the I-V curve with increase in nanotube diameter. The relative importance of these three phenomena depends on the energy, potential profile, and nanotube diameter.

Metal-Nanotube Coupling

In many experiments, nanotubes and metal couple by weak distributed coupling over the side wall over many unit cells of the nanotube [10, 11, 17, 18]. In this case details such as the diameter and chirality of the nanotube, Fermi wavevector of the metal, area of contact, and details of the metal-nanotube contact will play a role in determining the

transmission properties. We discuss some of these issues here. The formalism has been discussed in Ref.19: The metal electrode has a rectangular cross section in the (x,y) plane and is infinite in the z –direction (Fig. 5). The nanotube lies on the metal electrode and is stretched out in the circumferential direction. The Hamiltonian of the nanotube however reflects the periodic boundary conditions that yield the nanotube band structure.

If the metal and nanotube make uniform contact over several unit cells, wave vector conservation along the axial direction of the nanotube is enforced. However, the wave vector conservation along the circumferential direction is relaxed because of the finite extent of contact with the metal. The band structure of the nanotube yields that the axial wave vector corresponding to E = 0 are $2\pi/3a_0$ (0) and 0 for armchair and zigzag tubes respectively [4]. As a result, the threshold value of Fermi wave vector below which coupling between an armchair (zigzag) nanotube and metal is poor is $2\pi/3a_0$ (0). As the diameter of the nanotube increases and the contact length with the metal increases in the circumferential direction, wave vector conservation along the circumference also becomes important.

Fig. 6 shows the transmission probability from metal to armchair nanotube as a function of contact length. The units of contact length is number of nanotube unit cells, and the Fermi wavevector of metal (k_f) is shown for each case. The transmission does not increase with contact length for $k_f = 0.75\text{Å}^{-1}$. This is because axial wavevector conservation requires the metal to have a minimum wavevector of $2\pi/3a_0 = 0.85\text{Å}$ to couple to nanotubes at energies close to E=0. For larger k_f, the transmission probability

increases with increase in contact length. The transmission probability versus contact length of zigzag tubes (Fig. 7) have two differences from armchair tubes. The first point is that there is no threshold Fermi wavevector of the metal below which the nanotube does not couple to the metal. This is shown in the $k_f = 0.4\text{Å}^{-1}$ case, where the transmission monotonically increases with contact length, in contrast to the $k_f = 0.75\text{Å}^{-1}$ case of armchair nanotubes. A threshold k_f is absent for zigzag nanotubes because the sub-bands at $E = 0$ cross at $k = 0$. The second point is that for $k_f = 1.2\text{Å}$ (Fermi wavevector for gold), the transmission probability is smaller than the corresponding armchair case. This is because the nanotube wavevector in the circumferential direction (k_c) of metallic zigzag tubes is large. $k_c = 4\pi/3a_0 = 1.7\text{Å}$ for the crossing bands and as a result, the overlap integral in the Born approximation, $\langle \Psi_c \mid H_{c\text{-}m} \mid \Psi_m \rangle$ is small. Ψ_m and Ψ_c are the metal and nanotube wave functions, and $H_{c\text{-}m}$ represents the nanotube-metal coupling.

The transmission probability increases monotonically with contact length as seen in the experiments of references 11 and 17 (Figs. 5 and 6). This dependence arises because in the limit of weak metal-nanotube coupling, increase in contact length results in an increase in the transition probability to scatter from metal to nanotube. The transmission will saturate at large contact lengths as there are only two conducting sub-bands at the band center. In contrast, in the limit of strong nanotube-metal coupling, the transmission probability will reach its maximum by contacting only a few layers along its length. In both Figs. 6 and 7, the transmission probability increases with increase in k_f. This feature arises because electrons with a wavevector component along the nanotube axis that is larger than $2\pi/3a_0$ (0) for armchair (zigzag) nanotubes can scatter from the metal to

nanotube, and a larger k_f implies a large number of available metal electron states. So, from this view point it can be concluded that a larger metal Fermi wave vector is more desirable for the purpose of contacts to nanotubes [20]. For the purpose of these calculations, we considered a (2,2) armchair tube and a (3,0) zigzag nanotube. The essential physics is in principle true for larger diameter nanotubes also.

Concluding Remarks

We have provided a brief overview of the expected role of carbon nanotubes in future nanoelectronics. The key to device development is the controlled growth of nanotubes on patterned substrates with control over diameter and chirality. Catalyst preparation is critical to achieve the controlled growth. We have demonstrated physical sputtering of transition metals on patterns to be a viable technique in preparation of nanotubes. We have also presented some theoretical aspects of transport in nanotubes. We calculated the ballistic current through a carbon nanotube by neglecting electron-phonon and electron-electron interactions. We find that the current carrying capacity of metallic carbon nanotube wires is limited by the current flow through the non crossing subbands. Electrons injected in the non crossing subbands are primarily Bragg reflected. As the diameter of the nanotube increases Zener tunneling can contribute to current because the energy barrier for tunneling becomes smaller (ΔE_{NC} decreases as inverse diameter). Metal-nanotube coupling exhibits an interesting behavior with chirality. The physics of this behavior lies in the variation of wave vector corresponding to E=0, with chirality. As a result, the threshold Fermi wave vector of a metal contact is 0.85 and 0 inverse

Angstroms for armchair and zigzag nanotubes respectively. We also find that at a Fermi wave vector of 1.2 inverse Angstrom (gold), an armchair tube couples better than a zigzag tube to a metal. This behavior arises because of the larger momentum in the circumferential direction in the case of zigzag nanotubes.

References

1. See http://www.nano.gov to learn more about nanotechnology.
2. Ph. Avouris, T. Hertel, R. Martel, T. Schmidt, H.R. Shea, and R.E. Walkup, Appl. Surf. Sci., **141**, 201 (1999).
3. Y. Saito, K. Hamaguchi, S. Uemura, K. Uchida, Y. Tasaka, F. Ikazaki, M. Yumura, A. Kasuya, and Y. Nishina, Appl. Phys. A, **67**, 95 (1998).
4. M.S. Dresselhaus, G. Dresselhaus, and P.C. Eklund, Science of fullerenes and carbon nanotubes, Academic Press, San Diego, (1996).
5. L. Yang, M. Anantram, J. Han, and J.P. Lu, Phys. Rev. B, **60**, 13874, (1999).
6. M.P. Anantram, and T.R. Govindan, Phys. Rev. B, **58**, 4882, (1998).
7. M. Menon and D. Srivastava, Phys. Rev. Lett., **79**, 4453, (1997).
8. C. Papadopoulos, A. Ratikin, J. Li, A.S. Vedeneiv, and J. M. Xu, Phys. Rev. Lett, **85**, 3476 (2000).
9. S.J. Tans, A.R.M. Verschueren, and C. Dekker, Nature, **393**, 49, (1998).
10. R. Martel, T. Schmidt, H.R. Shea, T. Hertel, and Ph. Avouris, Appl. Phys. Lett., **73**, 2447, (1998).
11. S. Frank, P. Poncharal, Z. L. Wang and W. A. de Heer, Science **280**, 1744 (1998).
12. P. J. de Pablo, E. Graugnard, B. Walsh, R. P. Andres, S. Datta and R. Reifenberger, Appl. Phys. Lett. **74**, 323 (1999).

13. J. Kong, H.T. Soh, A.M. Cassell, C.F. Quate and H. Dai, Nature, **395**, 878, (1998).

14. L. Balents and M. P. A. Fisher, Phys. Rev. B **55**, R11973, (1997); Y. A. Krotov, D. H. Lee and S. G. Louie, Phys. Rev. Lett. **78**, 4245, (1997).

15. M. F. Lin and D. S. Chuu, Phys. Rev. B, **56**, 4996 (1997); D. Esfarjani, A. A. Farajian, Y. Hashi and Y. Kawazoe, Appl. Phys. Lett., **74**, 79 (1999); F. Leonard and J. Tersoff, Preprint.

16. M. P. Anantram, Phys. Rev. B **62**, 4837 (2000).

17. S. J. Tans, M. Devoret, H. Dai, A. Thess, R.E. Smalley, L.J. Geerligs and C. Dekker, Nature **386**, 474 (1997).

18. D. H. Cobden, M. Bockrath, P. L. McEuen, A. G. Rinzler and R. E. Smalley, Phys. Rev. Lett **81**, 681 (1998); C. Schonenberger, A. Bachtold, C. Strunk, J.-P. Salvetat and L. Forro, Appl. Phys. A: Mater. Sci. Process, **A69**, 283 (1999).

19. M. P. Anantram, S. Datta, Y. Xue, Phys. Rev. B, **61**, 14219 (2000).

20. J. Tersoff, Appl. Phys. Lett. **74**, 2122 (1999).

Figure Captions

Fig. 1: TEM image of a single wall nanotube grown by CVD

Fig. 2: (a) The current versus voltage of a 1000 Å long (10,10) armchair nanotube when the applied voltage drops uniformly across the nanotube. (b) The differential conductance is smaller than $4e^2/h$ even though electrons are injected into a large number of sub-bands at higher energies.

Fig. 3: Each rectangular box is a plot of energy versus wavevector with the sub-band bottom equal to the electrostatic potential in that section. Only a few sub-bands are shown for the sake of clarity. This plot aids in understanding the results in Figs. 2 and 4. The crossing sub-bands which are transmitted contribute to current. The contribution to current by the non crossing sub-bands is determined by the competition between Bragg reflection and Zener type tunneling.

Fig. 4: The current versus voltage in the case of a 1000 Å long (20,20) nanotube for $L_{sc} = 10$ and 100 in Eq. (1). Note that for the smaller screening length (L_{sc}), Zener tunneling contributes to current and so the I-V characteristic deviates from the $L_{sc} = 100$ case and the solid line of Fig. 2.

Fig. 5: Nanotube lying on a metal contact. The length of the metal contact along the z-direction is infinitely long (open boundaries).

Fig. 6: Plot of transmission probability versus contact length between metal and armchair nanotube, for three different values of the metal Fermi wavevector (k_f).

Fig. 7: Same as Fig. 6 but for zigzag nanotubes.

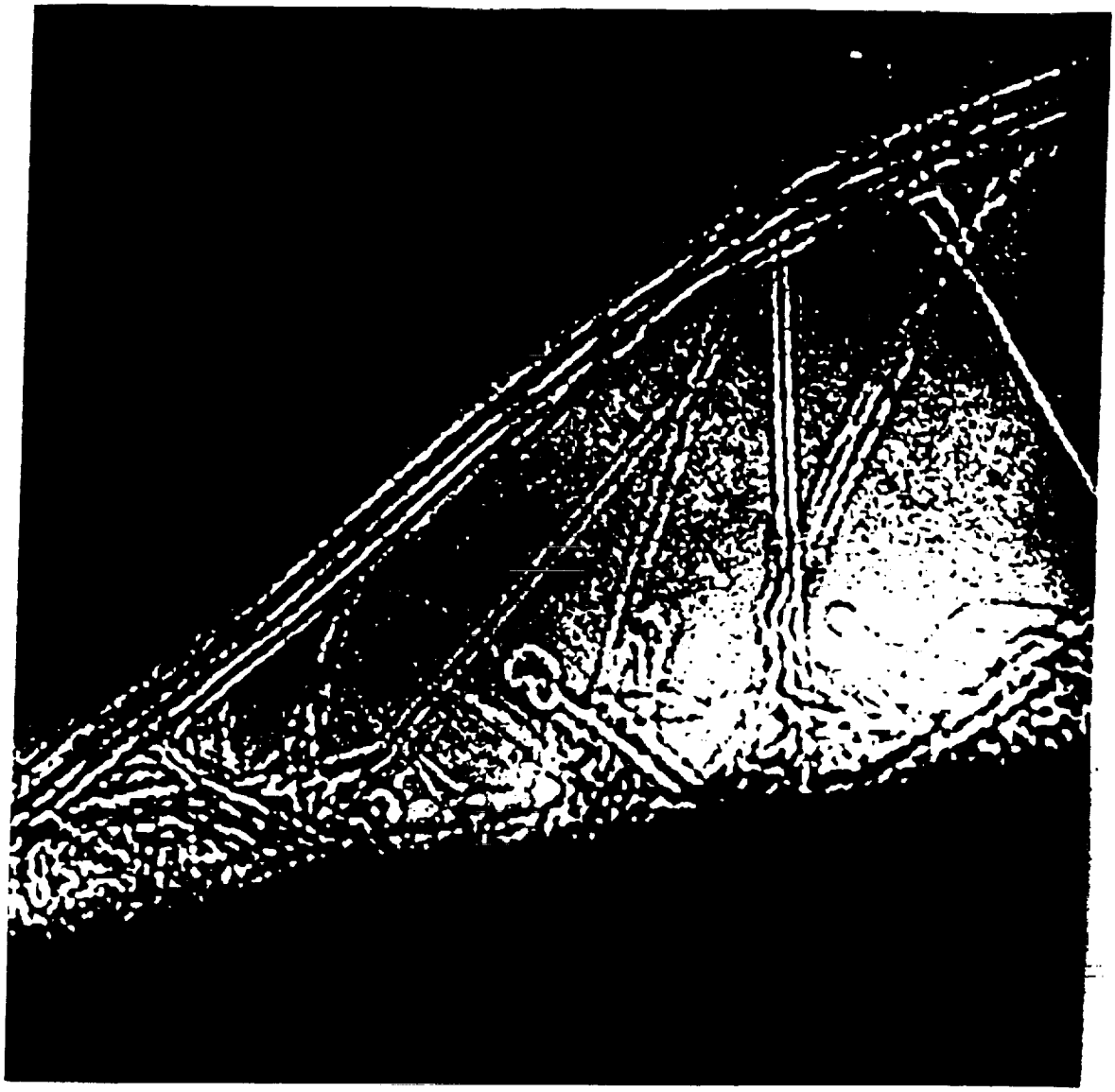

Fig. 1

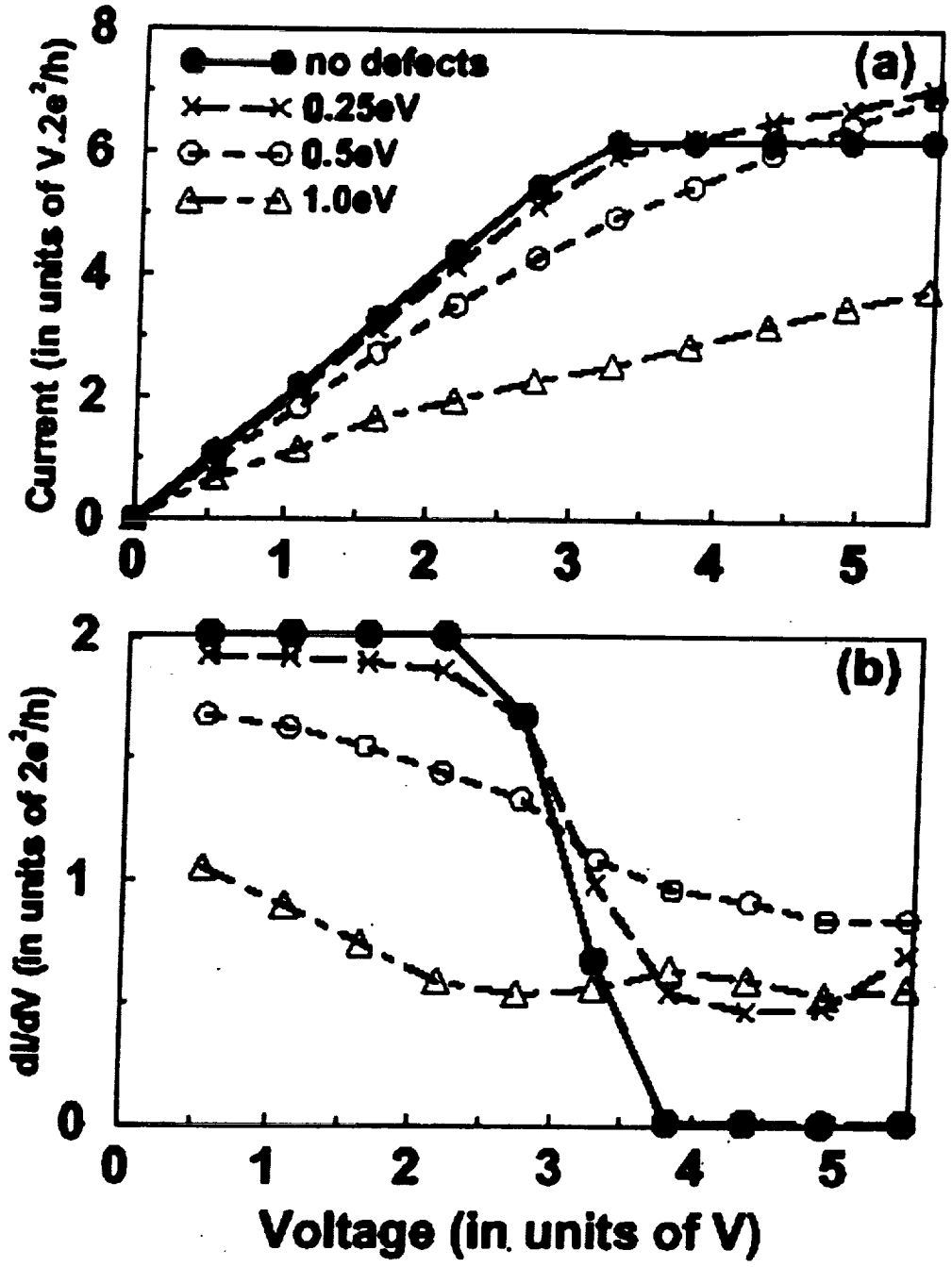
no defects
0.25eV
0.5eV
1.0eV
(a)
Current (in units of V.2e²/h)
(b)
dI/dV (in units of 2e²/h)
Voltage (in units of V)

Fig. 2.

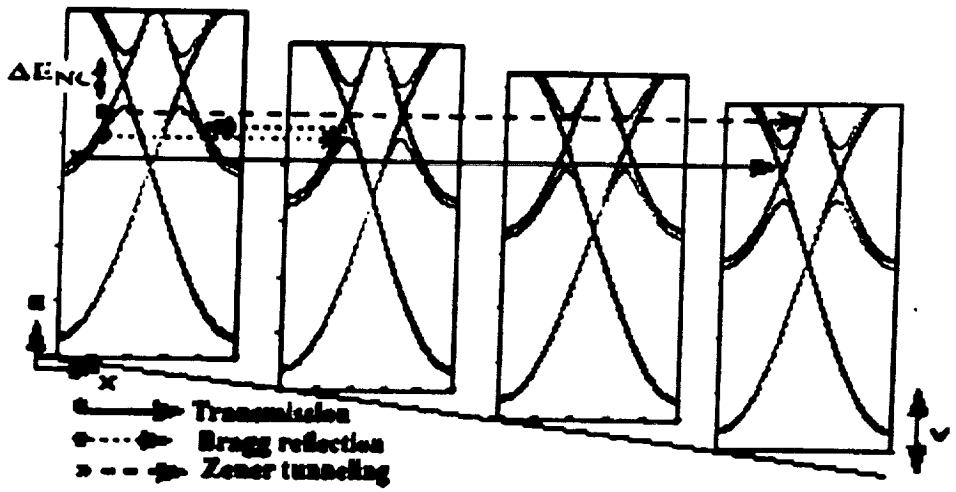
Transmission
Bragg reflection
Zener tunneling

Fig. 3.

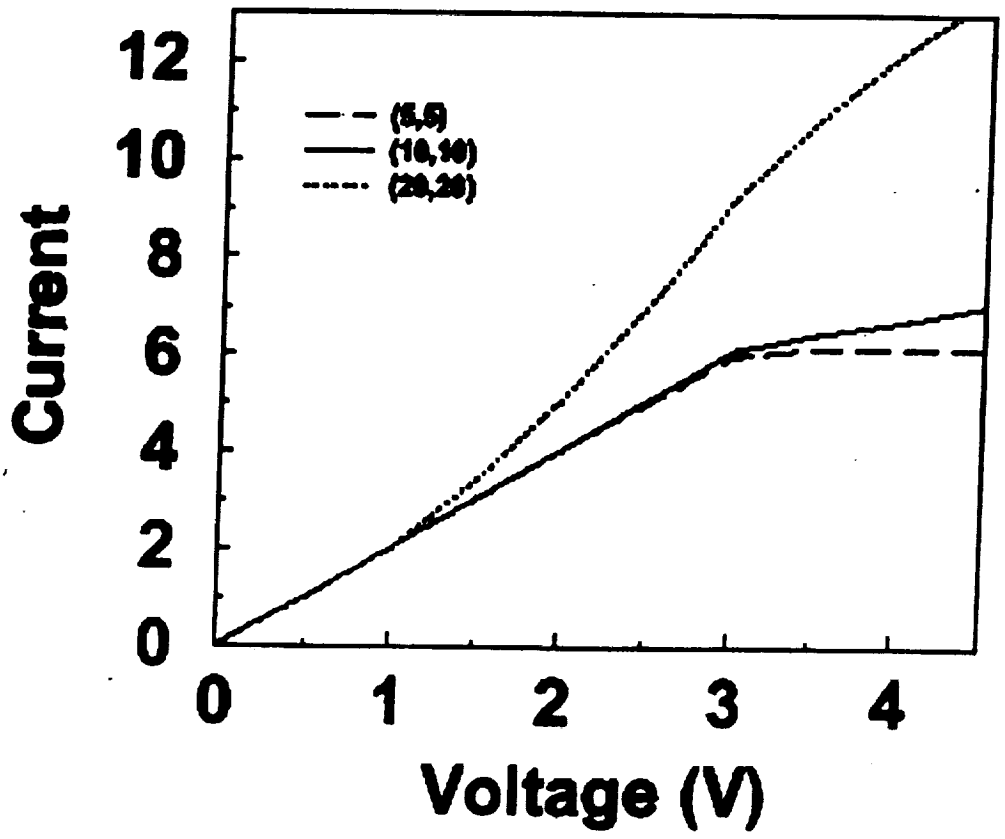
Current
Voltage (V)
0
2
4
6
8
10
12
0
1
2
3
4

Fig. 4.

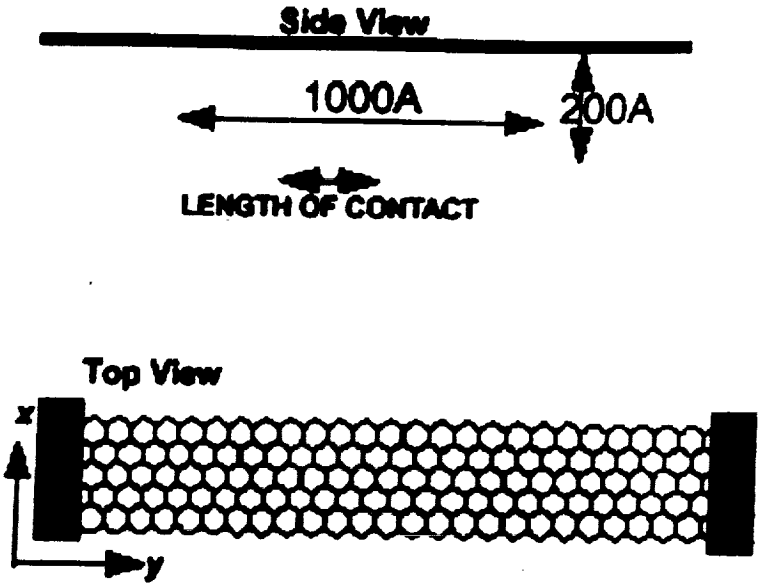
Side View
1000A
200A
LENGTH OF CONTACT
Top View
x
y

Fig. 5.

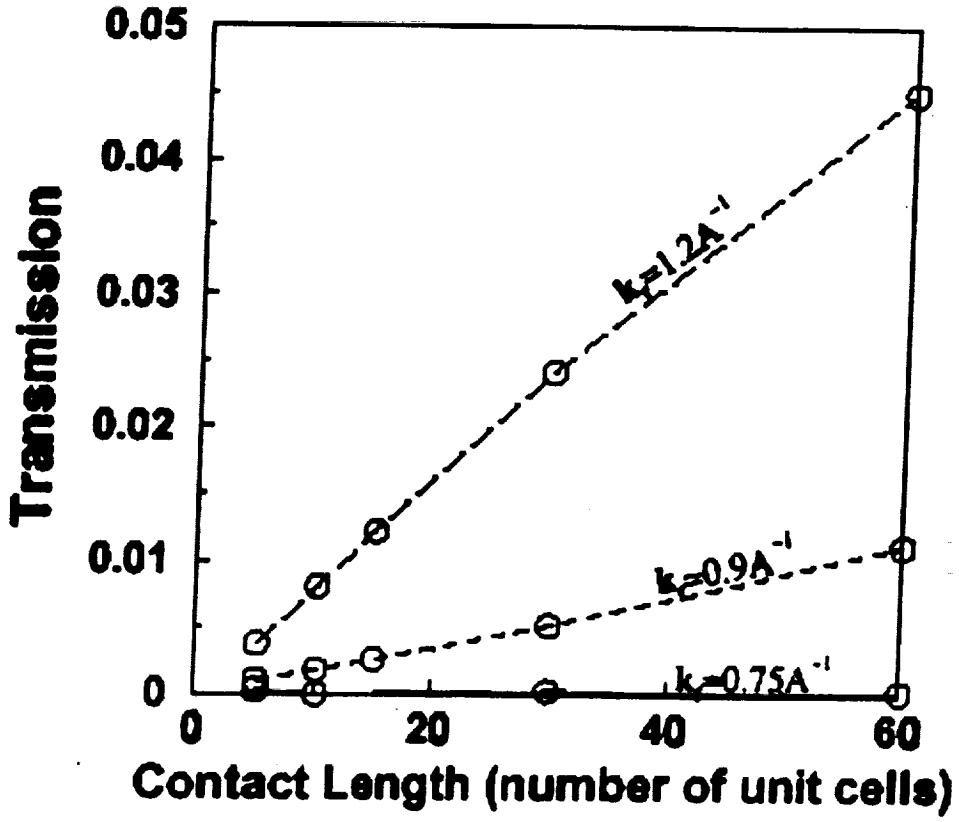
0.05
0.04
0.03
0.02
0.01
0
Transmission
0
20
40
60
Contact Length (number of unit cells)
k=1.2A-1
k=0.9A-1
k=0.75A-1

Fig. 6.

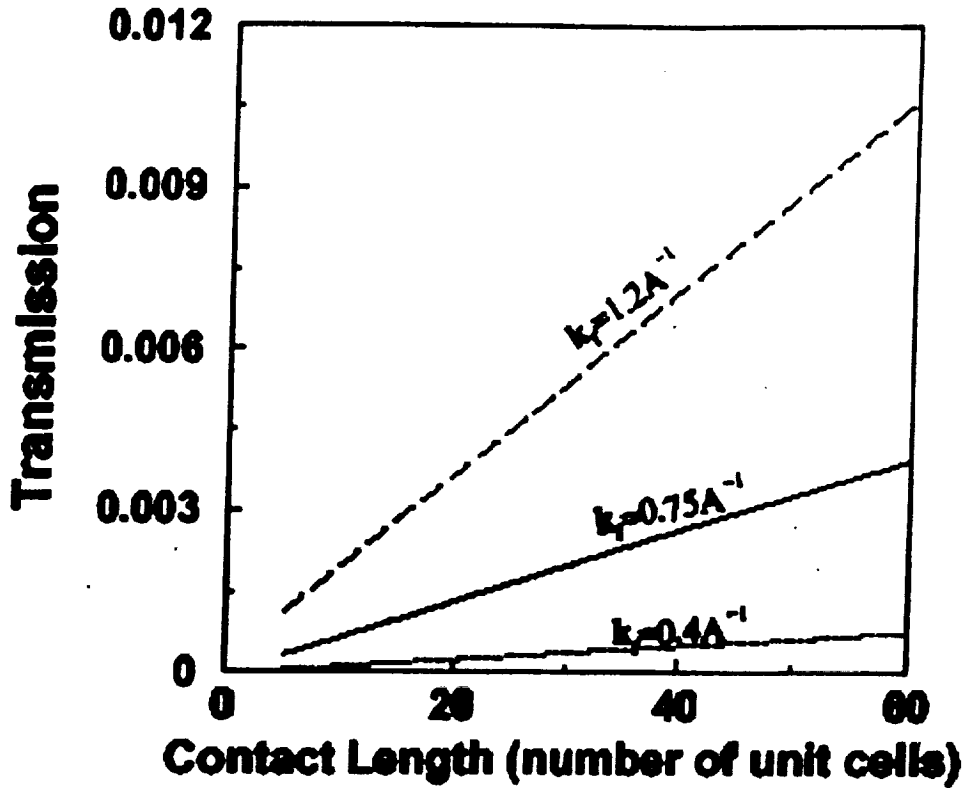
0.012
0.009
0.006
0.003
0
Transmission
0
20
40
60
Contact Length (number of unit cells)
k=1.2A^-1
k=0.75A^-1
k=0.4A^-1

Fig. 7.